

This discussion paper is/has been under review for the journal Geoscientific Model Development (GMD). Please refer to the corresponding final paper in GMD if available.

PRACTISE – Photo Rectification And ClassificaTion SoftwarE (V.1.0)

S. Härer¹, M. Bernhardt¹, J. G. Corripio², and K. Schulz¹

¹Department of Geography, LMU Munich, Germany

²meteoexploration.com, Innsbruck, Austria

Received: 28 November 2012 – Accepted: 8 January 2013 – Published: 18 January 2013

Correspondence to: S. Härer (s.haerer@iggf.geo.uni-muenchen.de)

Published by Copernicus Publications on behalf of the European Geosciences Union.

GMDD

6, 171–202, 2013

**PRACTISE – Photo
Rectification And
ClassificaTion
SoftwarE (V.1.0)**

S. Härer et al.

[Title Page](#)

[Abstract](#)

[Introduction](#)

[Conclusions](#)

[References](#)

[Tables](#)

[Figures](#)

[⏪](#)

[⏩](#)

[◀](#)

[▶](#)

[Back](#)

[Close](#)

[Full Screen / Esc](#)

[Printer-friendly Version](#)

[Interactive Discussion](#)



Abstract

Terrestrial photography is a cost-effective and easy-to-use method to derive the status of spatially distributed land surface parameters. It can be used to continuously investigate remote and often inaccessible terrain. We focus on the observation of snow cover patterns in high mountainous areas. The high temporal and spatial resolution of the photographs have various applications, e.g. validating spatially distributed snow hydrological models. However, a one to one analysis of projected model results to photographs requires a preceding georectification of the digital camera images. To accelerate and simplify the analysis, we have developed the “Photo Rectification And Classification Software” (PRACTISE) that is available as a Matlab code. The routine requires a digital camera image, the camera location and its orientation, as well as a digital elevation model (DEM) as input. In case of an unknown viewing orientation an optional optimisation routine using ground control points (GCPs) helps to identify the missing parameters. PRACTISE also calculates a viewshed using the DEM and the camera position and it projects the visible DEM pixels to the image plane where they are subsequently classified. The resulting projected and classified image can be directly compared to other projected data and can be used within any geoinformation system. The Matlab routine was tested using observations of the north western slope of the Schneefernerkopf, Zugspitze, Germany. The obtained results have shown that PRACTISE is a fast and user-friendly tool, able to derive the microscale variability of snow cover extent in high alpine terrain, but can also easily be adapted to other land surface applications.

1 Introduction

Oblique terrestrial photography has become a frequently used observation method in various research disciplines, such as vegetation phenology (Richardson et al., 2007; Ahrends et al., 2008; Crimmins and Crimmins, 2008; Migliavacca et al., 2011), land

GMDD

6, 171–202, 2013

PRACTISE – Photo Rectification And Classification Software (V.1.0)

S. Härer et al.

[Title Page](#)

[Abstract](#)

[Introduction](#)

[Conclusions](#)

[References](#)

[Tables](#)

[Figures](#)

[⏪](#)

[⏩](#)

[◀](#)

[▶](#)

[Back](#)

[Close](#)

[Full Screen / Esc](#)

[Printer-friendly Version](#)

[Interactive Discussion](#)



PRACTISE – Photo Rectification And Classification Software (V.1.0)

S. Härer et al.

[Title Page](#)

[Abstract](#)

[Introduction](#)

[Conclusions](#)

[References](#)

[Tables](#)

[Figures](#)



[Back](#)

[Close](#)

[Full Screen / Esc](#)

[Printer-friendly Version](#)

[Interactive Discussion](#)

cover studies (Clark and Hardegree, 2005; Zier and Baker, 2006; Roush et al., 2007; Michel et al., 2010) and volcanology (Major et al., 2009). Here, we focus on glaciology and snow hydrology where for example investigations of the snow albedo on glaciers were realised by Corripio (2004), Rivera et al. (2008) and Dumont et al. (2009). For a comprehensive overview on snow fall interception of vegetation, glacier velocity and snow cover mapping, we refer to Parajka et al. (2012). The frequent application of terrestrial photography in glaciology and snow hydrology is related to the fact that field campaigns and satellite-based remote sensing have limitations due to the prevailing weather conditions and the complexity of mountainous terrain (Klemes, 1990). However, the observation of patterns of land surface characteristics and, in particular, snow cover distributions become more and more important under the topic of climate change research (Schulz et al., 2006; Bavay et al., 2009). Terrestrial photography offers an easy-to-use and inexpensive opportunity to investigate these patterns, even in remote areas.

With the increasing availability of cost-effective high-resolution digital cameras and high-resolution digital elevation models, new tools can be developed to observe and map the patterns of land surface variables such as the spatial distribution of the snow cover in mountainous terrain. This is challenging due to the central projection and the almost horizontal recording angle that is inherent in terrestrial photography. Tools, developed by Aschenwald et al. (2001) and Corripio (2004), addressed this problem by projecting the DEM to the camera image plane. Aschenwald et al. (2001) used a photogrammetric approach that needs various ground control points (GCPs) for the georectification process. This however is unfavourable in remote, mountainous terrain where the derivation of GCPs can be time-consuming and costly. Additionally, the integrated optimisation procedure in their approach only optimises the camera target position T , i.e. the center position of the photograph whereas all other parameters remain fixed. The georectification method applied in Corripio (2004) is based on an animation and rendering technique by Watt and Watt (1992). This method solely needs one GCP (T), but 13 camera parameters have to be set manually. If the first guess of these

parameters is incorrect, they have to be corrected by changing them in an iterative way, which is unfavourable if extensive time series have to be processed.

The Photo Rectification And Classification Software (PRACTISE) introduced here is based on the approach of Corripio (2004) but has been optimized and extended by additional model features. We use slightly different formulations for the calculation of the 3-D rotation and projection. Even more importantly, several new optional routines are implemented in PRACTISE. This includes the dynamically dimensioned search (DDS) algorithm (Tolson and Shoemaker, 2007) to automatically identify the camera location and orientation and an integrated viewshed algorithm (Wang et al., 2000). The inclusion of the viewshed algorithm simplifies the visibility analysis by computing the viewshed generation directly without the additional step of using a geoinformation system, as is needed when using other georectification routines. PRACTISE also obtains an automatic and a manual snow classification algorithm and in addition, a bulk mode is implemented, i.e. several images can be classified in one program evaluation. The Matlab source code is freely available and even though it is designed to classify the snow variability in mountainous terrain, it can be easily adapted to other fields of research, e.g. greenness indexes in phenology (Richardson et al., 2007; Ahrends et al., 2008; Crimmins and Crimmins, 2008; Migliavacca et al., 2011).

2 Data

The test area for PRACTISE is located near the Zugspitze mountain in the Alps (located in Bavaria, Germany, Fig. 1a). A common single lens reflex camera (SLR, Canon EOS 550D, Canon EF 17–40 mm f/4L USM objective lens) was installed at 2665 m a.s.l. at the Environmental Research Station Schneefernerhaus (UFS, 5th floor) which is located on the south slope of the Zugspitze. The camera was oriented towards the test area, on the northeast facing slope of the Schneefernerkopf summit (21.1 ha, Fig. 1b). The skiing area on the glacier was excluded. During daylight, hourly images were taken from 10 May 2011 to 2 March 2012, however some technical problems with the automatic

PRACTISE – Photo Rectification And Classification Software (V.1.0)

S. Härer et al.

[Title Page](#)

[Abstract](#)

[Introduction](#)

[Conclusions](#)

[References](#)

[Tables](#)

[Figures](#)



[Back](#)

[Close](#)

[Full Screen / Esc](#)

[Printer-friendly Version](#)

[Interactive Discussion](#)



timer reduced the number of photographs taken to 2061. The hourly frequency increased the probability to retrieve at least one suitable picture per day, independently of the weather conditions.

PRACTISE requires a DEM raster and the outer camera properties, i.e. the viewpoint C , the camera target position T and the rolling angle ξ of the camera, as inputs. C and T are determined by using latitude and longitude, as well as the altitude derived from the corresponding DEM pixel. If necessary, a camera offset o (installation height above the surface) is added to the altitude of C and referred to as C_o . Additionally, inner camera properties are necessary, such as the focus length f , as well as the sensor (CCD or CMOS) dimensions: height h and width w .

We selected 3 photographs to show the functionality of PRACTISE, and to display different recording situations, i.e. different weather conditions and snow cover extents. The camera image taken on 11 May 2011 at 08:15 a.m. (Fig. 1b) represented the start of the ablation period in spring under clear sky conditions. The photograph from 16 August 2011, 11:05 a.m., was recorded under clear sky conditions in summer with almost no snow in the investigation area, whereas the photograph from 17 February 2012 at 03:07 p.m. described cloudy conditions directly after a snowfall event in winter.

The input given for the georectification and the classification of the photographs is presented in Table 1. All camera dependent parameters were taken from the user manual of the Canon camera system. Using the best resolution (17.9 Mpx), the pixel dimensions of the photographs are vertically 3456 px (N_v) and horizontally 5184 px (N_h). The latitude and longitude positions of C and T were visually derived from an official orthophoto from 2009 with a spatial resolution of 0.2 m provided by the Bavarian State Office for Survey and Geoinformation. The DEM had a spatial resolution of 1 m and originated from an airborne laser scanning campaign in 2006 by the Martin Luther University Halle-Wittenberg. The parameters o , ξ and f were estimated after the installation of the camera system. The GCPs of each photograph were determined by using the orthophoto in combination with the DEM for the longitude, latitude and altitude as well as the photograph with the row and column information.

PRACTISE – Photo Rectification And Classification Software (V.1.0)

S. Härer et al.

[Title Page](#)

[Abstract](#)

[Introduction](#)

[Conclusions](#)

[References](#)

[Tables](#)

[Figures](#)



[Back](#)

[Close](#)

[Full Screen / Esc](#)

[Printer-friendly Version](#)

[Interactive Discussion](#)



3 Model routines

PRACTISE is programmed in Matlab and divided into four modules that are presented in the following sections. The modular structure facilitates to switch routines on and off or even to exchange single modules. In the default case, PRACTISE starts with the viewshed generation (Sect. 3.1). Subsequently, the georectification procedure is applied (Sect. 3.2) and finally, the snow classification is executed (Sect. 3.4). If all routines are activated PRACTISE launches the accuracy assessment of the GCPs first and computes the deviations between assumed and real position (Sect. 3.3). Afterwards, the DDS algorithm optimises the outer and inner camera orientation (Sect. 3.3), and then the default procedure starts again. In each section, we will show the processing steps based on the photograph of 11 May 2011 at 08.15 a.m. (Fig. 1b).

3.1 Viewshed

In a first step, PRACTISE identifies the pixels of the DEM, which are visible from the camera location. This is necessary because pixels of the digital image can only be attributed to those DEM pixels. It should be considered that the spatial resolution of the DEM determines the detail of the results. The implemented viewshed calculation is an optional feature that can be bypassed if external data is provided.

The viewshed generation is based on the “reference planes” concept (Wang et al., 2000) and requires a DEM raster and the camera position C_o . By definition, only the horizontal centres of pixels are utilized in the visibility analysis. The viewshed calculation is divided into eight main directions (N, NE, E, SE, S, SW, W and NW) and eight sectors which are defined over the main directions (Fig. 2a).

The algorithm starts the visibility analysis at the DEM pixels in the second ring and proceeds stepwise to the cells of the outer rings (Fig. 2a). All pixels in the first ring are assumed to be visible, since no obstacles to the viewpoint were evident. The general functionality of the method is shown by using the example of the west-northwest (W-NW) sector (shaded area in Fig. 2a, b).

GMDD

6, 171–202, 2013

PRACTISE – Photo Rectification And Classification Software (V.1.0)

S. Härer et al.

[Title Page](#)

[Abstract](#)

[Introduction](#)

[Conclusions](#)

[References](#)

[Tables](#)

[Figures](#)



[Back](#)

[Close](#)

[Full Screen / Esc](#)

[Printer-friendly Version](#)

[Interactive Discussion](#)



PRACTISE – Photo Rectification And Classification Software (V.1.0)

S. Härer et al.

[Title Page](#)

[Abstract](#)

[Introduction](#)

[Conclusions](#)

[References](#)

[Tables](#)

[Figures](#)

[⏪](#)

[⏩](#)

[◀](#)

[▶](#)

[Back](#)

[Close](#)

[Full Screen / Esc](#)

[Printer-friendly Version](#)

[Interactive Discussion](#)

In a first step, the elevation of the coordinate system is modified by setting the elevation of C_o to zero. The normalised camera position at row i and column j of the DEM raster simplifies the plane generation and is hereinafter referred to as $s_{i,j}$ (Fig. 2a, b). Then, three pixel values define the plane which builds the criteria of visibility (Z) for the destination point $d_{m,n}$ (Fig. 2b). These pixels are the normalised viewpoint $s_{i,j}$ as well as the neighbouring pixels $r_{m,n+1}$ and $r_{m+1,n+1}$. Both, $r_{m,n+1}$ and $r_{m+1,n+1}$, lie on the adjacent inner ring of $d_{m,n}$, e.g. the third ring in Fig. 2b. Additionally, these two points have the shortest distance to $s_{i,j}$ and to $d_{m,n}$ on that ring. The values of $r_{m,n+1}$ and $r_{m+1,n+1}$ represent the maximum height of either the normalized elevation at this raster position or, in relative terms, higher obstacles in the already calculated inner rings in between to $s_{i,j}$.

Z is then derived using:

$$Z = -(m-i)(r_{m,n+1} - r_{m+1,n+1}) + \frac{(n-j)((m-i)(r_{m,n+1} - r_{m+1,n+1}) + r_{m,n+1})}{n+1-j}. \quad (1)$$

The calculation for the main directions is simplified since the reference plane (Eq. 1) can be reduced to a “reference line” (Eq. 2). This is shown for the NW diagonal:

$$Z = r_{m+1,n+1} \frac{i-m}{j-m-1}. \quad (2)$$

A pixel is considered as visible if

$$d_{m,n} > Z.$$

In this case $r_{m,n}$ is assigned to the value of $d_{m,n}$ for further calculations in the adjacent outer ring, otherwise the pixel is invisible and $r_{m,n}$ is set to the value of Z . The next visibility check will be executed at $d_{m-1,n}$ (Fig. 2b). Other directions and sectors are calculated in a similar way.

The algorithm of Wang et al. (2000) was developed to generate a 360 degree viewshed. Assuming a central projection of the camera lens, we use the viewing direction

as well as the horizontal and vertical field of view and thus only compute the areas depicted on the photographs. Here, we additionally need the camera target position T and the inner camera properties f , h and w . The viewing direction is set by connecting C_o and T . The inner camera properties are necessary to calculate the corresponding horizontal and vertical field of view. A maximum vertical viewing angle ϕ_v to the viewing direction can be calculated over:

$$\phi_v = \pm \arctan \left(\frac{\frac{1}{2}h}{f} \right). \quad (3)$$

The maximum horizontal viewing angle ϕ_h of the photograph is calculated by replacing the height h by the width w in Eq. (3). The vertical or horizontal orientation of a camera image might be different to the real world vertical or horizontal orientation due to ξ .

Figure 3 shows the viewshed in this case study.

3.2 Georectification

PRACTISE uses an animation and rendering technique to georectify the visible DEM pixels (Watt and Watt, 1992). The principle behind the georectification process is illustrated in Fig. 4. The camera produces a 2-D representation of the 3-D landscape. The oblique and two-dimensional image lacks depth information, therefore a direct back-calculation of the 2-D information into a 3-D landscape is impossible. An opportunity for calculating it is to generate a 2-D virtual camera image of the DEM while conserving the real world position of any pixel. The RGB values of the camera can then be assigned to the virtual 2-D image. Afterwards, any pixel with the attached RGB information is re-projected to its real world position.

The georectification is shown for a single DEM pixel, whereas all visible pixels are successively processed in the same way. Given the fact that the pixel is visible from

Title Page

Abstract

Introduction

Conclusions

References

Tables

Figures

⏪

⏩

◀

▶

Back

Close

Full Screen / Esc

Printer-friendly Version

Interactive Discussion



C_o , its centre point coordinates P_w are derived and saved in a vector:

$$P_w = \begin{bmatrix} P_{wx} \\ P_{wy} \\ P_{wz} \end{bmatrix} \quad (4)$$

The transformation of the real world coordinates of the DEM into the camera coordinate system is achieved by a translation of the origin of the coordinate system to the viewpoint C_o and a subsequent multiplication of the translated pixel coordinates with a rotation matrix:

$$P_t = \begin{bmatrix} P_{tx} \\ P_{ty} \\ P_{tz} \end{bmatrix} = \begin{bmatrix} P_{wx} \\ P_{wy} \\ P_{wz} \end{bmatrix} - \begin{bmatrix} C_{ox} \\ C_{oy} \\ C_{oz} \end{bmatrix}, \quad (5)$$

$$P_c = \begin{bmatrix} P_{cx} \\ P_{cy} \\ P_{cz} \end{bmatrix} = \begin{bmatrix} U_x & U_y & U_z \\ V_x & V_y & V_z \\ N_x & N_y & N_z \end{bmatrix} \begin{bmatrix} P_{tx} \\ P_{ty} \\ P_{tz} \end{bmatrix}. \quad (6)$$

The unit vectors U , V and N describe the axis of the new camera coordinate system (Fig. 5), where N points in the viewing direction. U and V are the horizontal and vertical axis of the camera system and create a plane that is parallel to the image plane (Figs. 4 and 5). The calculation of N is performed on the basis of the real world coordinates of C_o and T :

$$N = \frac{T - C_o}{|T - C_o|}. \quad (7)$$

Following Corripio (2004), we use cross products to calculate U and V (Fig. 5), if $N_z \neq 0$:

$$U = \begin{cases} N \times \frac{N_{xy}}{|N_{xy}|} & \text{for } N_z > 0 \\ \frac{N_{xy}}{|N_{xy}|} \times N & \text{for } N_z < 0 \end{cases}, \quad (8)$$

$$V = U \times N, \quad (9)$$

where $N_{xy} = [N_x, N_y, 0]$. We extend the calculation to the situation where $N = N_{xy}$, i.e. $N_z = 0$. In this particular case, we set $V = [0, 0, 1]$, and calculate U by computing the cross product of V and N .

In the case of the camera not being completely levelled, an additional rotation of the coordinates around N is required:

$$P_{Cr} = \begin{bmatrix} P_{Crx} \\ P_{Cry} \\ P_{Crz} \end{bmatrix} = \begin{bmatrix} \cos(\xi) & \sin(\xi) & 0 \\ -\sin(\xi) & \cos(\xi) & 0 \\ 0 & 0 & 1 \end{bmatrix} \begin{bmatrix} P_{Cx} \\ P_{Cy} \\ P_{Cz} \end{bmatrix} \quad (10)$$

where the rolling angle ξ is defined from 0° to $\pm 90^\circ$, where the positive values turn the U - V -plane in the viewing direction clockwise, and the negative values turn it anticlockwise.

The last step of the georectification is the projection of the rotated coordinates P_{Cr} to the image plane p . The three coordinate values of the DEM pixel determine the position in the camera space, where P_{Crx} as well as P_{Cry} hold the horizontal and vertical information and P_{Crz} the depth information. Different to Corripio (2004), we reduce the 3-D problem (P_{Cr} to P_p) to two 2-D problems; a horizontal (P_{Crx} to P_{px}) and a vertical (P_{Cry} to P_{py}) one. We solve each of them in two steps. At first, we directly apply the intercept theorem to calculate the horizontal (and vertical) component of the photograph at the CCD sensor plane s :

$$P_{sx} = \frac{P_{Crx}}{P_{Crz}} \cdot f, \quad (11)$$

Title Page

Abstract

Introduction

Conclusions

References

Tables

Figures

⏪

⏩

◀

▶

Back

Close

Full Screen / Esc

Printer-friendly Version

Interactive Discussion

where f is the focal length. P_{sy} is calculated by replacing P_{crx} with P_{cry} . It should be noted that the intercept theorem is applicable here, as T is located at $[0, 0, P_{crz}]$ in the camera coordinate system and thus lies in the centre of the photograph.

As a second step, P_{sx} and P_{sy} are scaled to the image plane p using the number of pixels N_h and N_v of the photograph in horizontal and vertical direction:

$$P_{px} = \frac{N_h}{\frac{1}{2}W} \cdot P_{sx}, \quad (12)$$

where w is the camera sensor width. P_{py} is computed in the same way but under usage of N_v and the CCD height h . Both, the photograph and the projected DEM are now in-plane. The last step is to shift the origin of the virtual camera image from $[N_h, /2, N_v /2]$ to the origin of the photograph $[0, 0]$. This is necessary as the photograph origin lies at the upper left corner while the projected DEM coordinate system is centred in the photograph. The overlay of the images facilitates the direct extraction of the RGB values for the classification which can be directly re-projected to the raster format of the DEM.

Figure 6 shows the overlay of the georectified DEM pixels and the photograph.

3.3 GCP accuracy assessment and DDS optimisation

If GCPs are available, PRACTISE offers an optional feature to optimise the outer and inner camera orientation used in the georectification procedure. The root mean square error (RMSE) is used as an error metric to determine the positional inaccuracy of the virtual camera image to the photograph. In most cases, this can be mainly attributed to an erroneous setting of the viewing direction and the camera properties.

We implemented a global optimization approach, the dynamically dimensioned search (DDS) algorithm (Tolson and Shoemaker, 2007), to minimise the displacement between observed and real location of the GCPs. We selected this technique as it reveals good results in a limited number of function evaluations (1000 to 10000). The general procedure of the implemented DDS algorithm is shown in Table 2.

PRACTISE – Photo Rectification And Classification Software (V.1.0)

S. Härer et al.

[Title Page](#)

[Abstract](#)

[Introduction](#)

[Conclusions](#)

[References](#)

[Tables](#)

[Figures](#)

[⏪](#)

[⏩](#)

[◀](#)

[▶](#)

[Back](#)

[Close](#)

[Full Screen / Esc](#)

[Printer-friendly Version](#)

[Interactive Discussion](#)

Within the optimisation procedure, 7 decision variables are optimised: the latitude and longitude of C and T , the camera offset o , the rolling angle ξ , and the focal length f . The latter is included in the optimisation as the actual and nominal focal length of a camera lens will probably differ slightly. The initial guesses of the decision variables x^0 are taken from the original input (Table 1). Additionally, the user has to define the upper and lower boundary (x^{\max} and x^{\min}) that span the range of reasonable values (Table 3). At last, the maximum number of function evaluations m is specified. 6 GCPs are used for the exemplary DDS optimisation.

The algorithm starts with the georectification of the GCPs using x^0 and creates an initial $x^{\text{best}} = x^0$. Then, x^{new} is randomly generated (Table 2) and if the recalculation of the $\text{RMSE}(x^{\text{new}})$ results in a lower RMSE than $\text{RMSE}(x^{\text{best}})$, x^{best} is updated with x^{new} . The optimisation procedure stops when the number of iterations is equal to m and subsequently starts the georectification of the DEM with the best camera orientation (Table 2). In this example, $m = 3000$ as no large improvement have been observed with more iterations. At least one recalculation is recommended to verify that the global optimum was found.

Figure 7 depicts the correct position of the 6 GCPs (green crosses) in comparison to the georectification of the GCPs before and after the DDS optimisation (red circles and dots).

3.4 Classification

Here we focus on the classification of snow cover even though the investigation of other land surface variables is possible and only needs slight adaptations of the respective routine. Two classification routines of different complexity can be used. The first is based on threshold values, which have to be manually derived by analysing the RGB values of the snow cover and of the surrounding environment in the photograph. The second is an automatic snow cover classification routine (Salvatori et al., 2011), that is able to hasten the classification procedure if a long time series has to be processed.

PRACTISE – Photo Rectification And Classification Software (V.1.0)

S. Härer et al.

[Title Page](#)

[Abstract](#)

[Introduction](#)

[Conclusions](#)

[References](#)

[Tables](#)

[Figures](#)



[Back](#)

[Close](#)

[Full Screen / Esc](#)

[Printer-friendly Version](#)

[Interactive Discussion](#)



The manual classification assigns pixels with RGB values above certain thresholds to snow, where the threshold value can be in between 0 and 255 if 8 bit data is used. Since we want to classify fresh snow (pure white), as well as old snow, which turns grey with time, and use recordings in diffuse lighting conditions, due to clouds, the predefined thresholds change from image to image, where they are often around 150 for all bands. Furthermore, snow is generally approximately equally reflective within the RGB bands, while the reflectance values of for example, light-coloured bare rocks are significantly lower in the blue band. Hence, we introduced a test that verifies if the spread between the RGB values of one pixel does not exceed a specified threshold (e.g. 10).

The automatic classification of Salvatori et al. (2011) incorporates a statistical analysis of the image by using a DN frequency histogram (Fig. 8a). The algorithm uses the blue band exclusively because of the assumption that it is representative for the other bands with respect to snow. In the presence of snow, the histogram usually shows a bimodal distribution. The first local minimum over or equal to 127 is selected as the snow threshold (Fig. 8a). The DN frequency histogram has to be smoothed for this analysis by using a moving average window of 5. This is done for removing single outliers, which might be mistakenly interpreted as local minima. Salvatori et al. (2011) defined the size of the moving window as well as of the minimum histogram threshold of the blue band, on the basis of about 300 images. The resulting classification is shown in Fig. 8b.

The layout of PRACTISE also allows for an inclusion of other routines, such as those of Hinkler et al. (2002), Corripio (2004), Corripio et al. (2004) or Schmidt (2007) and of already classified images.

4 Results and discussion

The functionality of PRACTISE will be shown in the test area of Schneefernerkopf, Zugspitze on the basis of 3 photographs which are hereinafter referred to as the May (11 May 2011 at 08:15 a.m.), the August (16 August 2011, 11:05 a.m.) and the

February (17 February 2012 at 03:07 p.m.) images. All of the described routines were used to compute the snow cover extent.

In the DDS optimisation, we found an initial RMSE of 67.82 px between the GCPs and the control points within the May photograph (Table 3, x^0). The error could be reduced to 4.42 px by using the optimised input (Table 3, x^{best}). The RMSE after the DDS optimisation for the August and February image are 6 px and 5.49 px, whereas the initial error values are 43.45 px and 92.91 px, respectively. The comparison of initial and optimised RMSE values illustrate that the position accuracy of the optimised input is at least 7-fold higher than the initial input. The mean RMSE of these 3 photographs (5.30 px) corresponds to 0.79 m for the mean distance of 1044.46 m between the camera viewpoint and the GCPs and is thus smaller than the spatial resolution of the DEM (1 m).

The visual investigation of the automatically classified photographs (Fig. 9a to c in chronological order) showed qualitatively a good agreement between automatically classified and visually observed snow covered area. The very good match of the Fig. 9a and c is valid for clear sky as well as for cloudy conditions. In Fig. 9b, limitations in the classification with respect to light-coloured bare rock could be observed in the August image. A small test area (11 701 m², black box in Fig. 9b) was selected within the investigation area where visually no snow could be detected and a very strong effect of the erroneous classification had been identified. The misclassification of limestone as snow amounted to 477 m² which corresponded to a relative error of 4.1 %.

The August photograph was also processed using the manual classification routine (Fig. 9d). The thresholds of the RGB bands were identical to the automatically derived classification threshold (169) in Fig. 9b. The maximum allowed spread between the 3 RGB values of one pixel was 10. Qualitatively, the visual investigation of the overlay of the photograph and the classification shows a good match for the investigation area. We investigated again the same small test area (black box in Fig. 9d). The misclassification is reduced to 100 m² (0.9 %) in comparison to the automatic classification, due

PRACTISE – Photo Rectification And Classification Software (V.1.0)

S. Härer et al.

[Title Page](#)

[Abstract](#)

[Introduction](#)

[Conclusions](#)

[References](#)

[Tables](#)

[Figures](#)

[⏪](#)

[⏩](#)

[◀](#)

[▶](#)

[Back](#)

[Close](#)

[Full Screen / Esc](#)

[Printer-friendly Version](#)

[Interactive Discussion](#)



to the light-coloured bare rock reflecting the blue band significantly weaker than the red and green bands.

The resulting snow cover maps of the 3 photographs are depicted in the Fig. 10a–c using the classification of Fig. 9a, d and c, respectively. We compared the derived snow cover extent of Fig. 10a, to the DEM, respective to the slope in more detail. More than 90 % of the areas free of snow on this date are located in steep terrain with slope angles above 35° (without figure). With the last snowfall being on 3 May 2011, this is reasonable due to gravitational snow redistribution (Bernhardt and Schulz, 2010). The snow cover extents in the investigation area (black dotted line) are in accordance with the time of the year, and amount to 9.4 ha on 11 May 2011, 1.3 ha on 16 August 2011 and 12.2 ha on 17 February 2012.

The present results reveal that PRACTISE, with its large number of features and its modular flexibility, is an efficient software tool to produce temporal and spatial high-resolution snow cover maps. All methods used are well-established and we have shown that the DDS optimisation as well as the classification routines produce high quality results for the 3 investigated photographs, e.g. the accuracy assessment is better than the spatial resolution of the DEM. Furthermore, the automatic classification works well in most cases while the manual classification can be used as an alternative classification routine under unfavourable conditions. The presented classification results confirm the well-known limitations in the snow classification using the visible spectrum (0.4–0.7 µm). Shadows are another possible source of uncertainty, however they do not have a great effect on the snow cover mapping here as the recording time was able to be controlled and was adjusted to a minimum of shading by choosing the day time (Dozier, 1989; Winther and Hall, 1999; Schmidt, 2007; Salvatori et al., 2011).

The fast and easy processing of PRACTISE might help to increase the efficiency of terrestrial photography either to validate spatially distributed snow hydrological models (Lehning et al., 2006) or to statistically analyse snow patterns influenced by the topography (Lehning et al., 2011). Future studies using PRACTISE will test the comparability of SLR images to other methods of snow cover detection and include long-term

PRACTISE – Photo Rectification And Classification Software (V.1.0)

S. Härer et al.

[Title Page](#)

[Abstract](#)

[Introduction](#)

[Conclusions](#)

[References](#)

[Tables](#)

[Figures](#)



[Back](#)

[Close](#)

[Full Screen / Esc](#)

[Printer-friendly Version](#)

[Interactive Discussion](#)



studies. A further topic of research will be the development of an automatic classification algorithm that is less prone to misclassifications of snow in digital camera images caused by clouds, shadows or light bare rock.

Supplementary material related to this article is available online at:
5 [http://www.geosci-model-dev-discuss.net/6/171/2013/
gmdd-6-171-2013-supplement.zip](http://www.geosci-model-dev-discuss.net/6/171/2013/gmdd-6-171-2013-supplement.zip).

Acknowledgement. The authors want to especially thank Thomas Werz who installed and maintained the digital camera at the Environmental Research Station Schneefernerhaus (UFS) during his master thesis and David Morche providing the DEM. We appreciate the computational support of Ben Müller. The work was supported by the UFS, the doctoral scholarship program “Deutsche Bundesstiftung Umwelt” (DBU) and the Helmholtz Research School “Mechanisms and Interactions of Climate Change in Mountain Regions” (MICMoR).
10

References

- Ahrends, H. E., Brügger, R., Stöckli, R., Schenk, J., Michna, P., Jeanneret, F., Wanner, H., and Eugster, W.: Quantitative phenological observations of a mixed beech forest in northern Switzerland with digital photography, *J. Geophys. Res.*, 113, G04004, doi:10.1029/2007jg000650, 2008.
15
- Aschenwald, J., Leichter, K., Tasser, E., and Tappeiner, U.: Spatio-temporal landscape analysis in mountainous terrain by means of small format photography: a methodological approach, *IEEE T. Geosci. Remote*, 39, 885–893, doi:10.1109/36.917917, 2001.
20
- Bavay, M., Lehning, M., Jonas, T., and Löwe, H.: Simulations of future snow cover and discharge in Alpine headwater catchments, *Hydrol. Process.*, 23, 95–108, doi:10.1002/Hyp.7195, 2009.
- Bernhardt, M. and Schulz, K.: SnowSlide: a simple routine for calculating gravitational snow transport, *Geophys. Res. Lett.*, 37, L11502, doi:10.1029/2010gl043086, 2010.
25

GMDD

6, 171–202, 2013

PRACTISE – Photo Rectification And Classification Software (V.1.0)

S. Härer et al.

Title Page

Abstract

Introduction

Conclusions

References

Tables

Figures



Back

Close

Full Screen / Esc

Printer-friendly Version

Interactive Discussion

PRACTISE – Photo Rectification And Classification Software (V.1.0)

S. Härer et al.

[Title Page](#)

[Abstract](#)

[Introduction](#)

[Conclusions](#)

[References](#)

[Tables](#)

[Figures](#)

[⏪](#)

[⏩](#)

[◀](#)

[▶](#)

[Back](#)

[Close](#)

[Full Screen / Esc](#)

[Printer-friendly Version](#)

[Interactive Discussion](#)



- Clark, P. E. and Hardegee, S. P.: Quantifying vegetation change by point sampling landscape photography time series, *Rangeland Ecol. Manage.*, 58, 588–597, doi:10.2111/04-111R2.1, 2005.
- Corripio, J. G.: Snow surface albedo estimation using terrestrial photography, *Int. J. Remote Sens.*, 25, 5705–5729, doi:10.1080/01431160410001709002, 2004.
- Corripio, J. G., Durand, Y., Guyomarc'h, G., Mérindol, L., Lecorps, D., and Puğliése, P.: Land-based remote sensing of snow for the validation of a snow transport model, *Cold Regions Sci. Technol.*, 39, 93–104, doi:10.1016/j.coldregions.2004.03.007, 2004.
- Crimmins, M. and Crimmins, T.: Monitoring plant phenology using digital repeat photography, *Environ. Manage.*, 41, 949–958, doi:10.1007/s00267-008-9086-6, 2008.
- Dozier, J.: Spectral signature of alpine snow cover from the Landsat Thematic Mapper, *Remote Sens. Environ.*, 28, 9–22, doi:10.1016/0034-4257(89)90101-6, 1989.
- Dumont, M., Arnaud, Y., Six, D., and Corripio, J. G.: Retrieval of glacier surface albedo using terrestrial photography, *Houille Blanche*, 102–108, doi:10.1051/Lhb/2009021, 2009.
- Hinkler, J., Pedersen, S. B., Rasch, M., and Hansen, B. U.: Automatic snow cover monitoring at high temporal and spatial resolution, using images taken by a standard digital camera, *Int. J. Remote Sens.*, 23, 4669–4682, doi:10.1080/01431160110113881, 2002.
- Klemes, V.: The modelling of mountain hydrology: the ultimate challenge, *IAHS Publ.*, 190, 29–43, 1990.
- Lehning, M., Völksch, I., Gustafsson, D., Nguyen, T. A., Stähli, M., and Zappa, M.: ALPINE3D: a detailed model of mountain surface processes and its application to snow hydrology, *Hydrol. Process.*, 20, 2111–2128, doi:10.1002/Hyp.6204, 2006.
- Lehning, M., Grünewald, T., and Schirmer, M.: Mountain snow distribution governed by an altitudinal gradient and terrain roughness, *Geophys. Res. Lett.*, 38, L19504, doi:10.1029/2011gl048927, 2011.
- Major, J. J., Dzurisin, D., Schilling, S. P., and Poland, M. P.: Monitoring lava-dome growth during the 2004–2008 Mount St. Helens, Washington, eruption using oblique terrestrial photography, *Earth Planet. Sci. Lett.*, 286, 243–254, doi:10.1016/j.epsl.2009.06.034, 2009.
- Michel, P., Mathieu, R., and Mark, A. F.: Spatial analysis of oblique photo-point images for quantifying spatio-temporal changes in plant communities, *Appl. Veget. Sci.*, 13, 173–182, doi:10.1111/j.1654-109X.2009.01059.x, 2010.
- Migliavacca, M., Galvagno, M., Cremonese, E., Rossini, M., Meroni, M., Sonnentag, O., Cogliati, S., Manca, G., Diotri, F., Busetto, L., Cescatti, A., Colombo, R., Fava, F., di

PRACTISE – Photo Rectification And Classification Software (V.1.0)

S. Härer et al.

[Title Page](#)

[Abstract](#)

[Introduction](#)

[Conclusions](#)

[References](#)

[Tables](#)

[Figures](#)

[⏪](#)

[⏩](#)

[◀](#)

[▶](#)

[Back](#)

[Close](#)

[Full Screen / Esc](#)

[Printer-friendly Version](#)

[Interactive Discussion](#)

- Celia, U. M., Pari, E., Siniscalco, C., and Richardson, A. D.: Using digital repeat photography and eddy covariance data to model grassland phenology and photosynthetic CO₂ uptake, *Agric. Forest Meteorol.*, 151, 1325–1337, doi:10.1016/j.agrformet.2011.05.012, 2011.
- Parajka, J., Haas, P., Kirnbauer, R., Jansa, J., and Blöschl, G.: Potential of time-lapse photography of snow for hydrological purposes at the small catchment scale, *Hydrol. Process.*, 26, 3327–3337, doi:10.1002/Hyp.8389, 2012.
- Richardson, A. D., Jenkins, J. P., Braswell, B. H., Hollinger, D. Y., Ollinger, S. V., and Smith, M. L.: Use of digital webcam images to track spring green-up in a deciduous broadleaf forest, *Oecologia*, 152, 323–334, doi:10.1007/s00442-006-0657-z, 2007.
- Rivera, A., Corripio, J. G., Brock, B., Clavero, J., and Wendt, J.: Monitoring ice-capped active Volcan Villarrica, southern Chile, using terrestrial photography combined with automatic weather stations and global positioning systems, *J. Glaciol.*, 54, 920–930, doi:10.3189/002214308787780076, 2008.
- Roush, W., Munroe, J. S., and Fagre, D. B.: Development of a spatial analysis method using ground-based repeat photography to detect changes in the alpine treeline ecotone, Glacier National Park, Montana, USA, *Arctic Antarctic Alpine Res.*, 39, 297–308, doi:10.1657/1523-0430(2007)39[297:doasam]2.0.co;2, 2007.
- Salvatori, R., Plini, P., Giusto, M., Valt, M., Salzano, R., Montagnoli, M., Cagnati, A., Crepez, G., and Sigismondi, D.: Snow cover monitoring with images from digital camera systems, *Ital. J. Remote Sens.*, 43, 137–145, doi:10.5721/ItJRS201143211, 2011.
- Schmidt, S.: Die reliefabhängige Schneedeckenverteilung im Hochgebirge. Ein multiskaliger Methodenverbund am Beispiel des Lötschentals (Schweiz), Ph.D. thesis, Faculty of math and natural sciences, University of Bonn, Bonn, Germany, 2007.
- Schulz, K., Seppelt, R., Zehe, E., Vogel, H. J., and Attinger, S.: Importance of spatial structures in advancing hydrological sciences, *Water Resour. Res.*, 42, W03S03, doi:10.1029/2005wr004301, 2006.
- Tolson, B. A. and Shoemaker, C. A.: Dynamically dimensioned search algorithm for computationally efficient watershed model calibration, *Water Resour. Res.*, 43, W01413, doi:10.1029/2005wr004723, 2007.
- Wang, J., Robinson, G. J., and White, K.: Generating viewsheds without using sightlines, *Photogramm. Eng. Remote S.*, 66, 87–90, 2000.
- Watt, A. and Watt, M.: *Advanced Animation and Rendering Techniques: Theory and Practice*, ACM Press, New York, 1992.

Winther, J. G. and Hall, D. K.: Satellite-derived snow coverage related to hydropower production in Norway: present and future, *Int. J. Remote Sens.*, 20, 2991–3008, 1999.

Zier, J. L. and Baker, W. L.: A century of vegetation change in the San Juan Mountains, Colorado: an analysis using repeat photography, *Forest Ecol. Manage.*, 228, 251–262, doi:10.1016/j.foreco.2006.02.049, 2006.

5

GMDD

6, 171–202, 2013

PRACTISE – Photo Rectification And ClassificaTion SoftwarE (V.1.0)

S. Härer et al.

Title Page

Abstract

Introduction

Conclusions

References

Tables

Figures



Back

Close

Full Screen / Esc

Printer-friendly Version

Interactive Discussion



Table 2. Working steps of the implemented DDS algorithm in PRACTISE (adapted from Tolson and Shoemaker, 2007).

	Define DDS inputs:
	Vector of initial solution $x^0 = [x_1, \dots, x_7]$
Step 1	Vectors of upper, x^{\max} , and lower, x^{\min} , boundaries for the 7 decision variables
	Maximum number of function evaluations m
	Neighbourhood perturbation size parameter r (0.2 is default)
Step 2	Set counter to 1, $i = 1$, and evaluate RMSE at initial solution $\text{RMSE}(x^0)$:
	$\text{RMSE}_{\text{best}} = \text{RMSE}(x^0)$, and $x^{\text{best}} = x^0$
	Randomly select J of the D decision variables for inclusion in neighbourhood $\{N\}$:
Step 3	Calculate probability each decision variable is included in $\{N\}$ as a function of the current iteration count: $P(i) = 1 - \ln(i)/\ln(m)$
	FOR $d = 1, \dots, D$ decision variables, add d to $\{N\}$ with probability P
	IF $\{N\}$ empty, select one random d for $\{N\}$
	FOR $j = 1, \dots, J$ decision variables in $\{N\}$, perturb x_j^{best} using a standard normal random variable $N(0, 1)$, reflecting at decision variable bounds if necessary:
Step 4	$x_j^{\text{new}} = x_j^{\text{best}} + \sigma_j N(0, 1)$, where $\sigma_j = r(x_j^{\max} - x_j^{\min})$
	IF $x_j^{\text{new}} < x_j^{\min}$, reflect perturbation: $x_j^{\text{new}} = x_j^{\min} + (x_j^{\min} - x_j^{\text{new}})$
	IF $x_j^{\text{new}} > x_j^{\max}$, set $x_j^{\text{new}} = x_j^{\max}$
	IF $x_j^{\text{new}} > x_j^{\max}$, reflect perturbation: $x_j^{\text{new}} = x_j^{\max} - (x_j^{\text{new}} - x_j^{\max})$ IF $x_j^{\text{new}} < x_j^{\min}$, set $x_j^{\text{new}} = x_j^{\min}$
	Evaluate $\text{RMSE}(x^{\text{new}})$ and update current best solution if necessary:
Step 5	IF $\text{RMSE}(x^{\text{new}}) \leq \text{RMSE}_{\text{best}}$, update new best solution: $\text{RMSE}_{\text{best}} = \text{RMSE}(x^{\text{new}})$ and $x^{\text{best}} = x^{\text{new}}$
	Update iteration count, $i = i + 1$, and check stopping criterion:
Step 6	IF $i = m$, STOP, print output ($\text{RMSE}_{\text{best}}$ and x^{best})
	ELSE go to Step 3

[Title Page](#)

[Abstract](#)

[Introduction](#)

[Conclusions](#)

[References](#)

[Tables](#)

[Figures](#)

[⏪](#)

[⏩](#)

[◀](#)

[▶](#)

[Back](#)

[Close](#)

[Full Screen / Esc](#)

[Printer-friendly Version](#)

[Interactive Discussion](#)



PRACTISE – Photo Rectification And Classification Software (V.1.0)

S. Härer et al.

Table 3. Vectors of the DDS optimisation example with 3000 iterations: \mathbf{x}^0 , \mathbf{x}^{\max} , \mathbf{x}^{\min} and \mathbf{x}^{best} . The values are in m except noted otherwise. \mathbf{x}^{\max} of \mathbf{C} is set to the values of \mathbf{x}_0 as the UFS building is represented in the DEM by a plateau. Hence, we confine the optimisation directions to stay at the edge or in front of the building. The latter needs a large camera offset to obtain the height of the 5th floor of the UFS.

	\mathbf{x}^0	\mathbf{x}^{\max}	\mathbf{x}^{\min}	\mathbf{x}^{best}
C_x	649 299.97	649 299.97	649 294.97	649 299.83
C_y	5 253 358.26	5 253 358.26	5 253 353.26	5 253 356.60
T_x	648 740.85	648 765.85	648 715.85	648 741.86
T_y	5 252 771.33	5 252 796.33	5 252 746.33	5 252 768.71
o	1.5	26.5	1	6.35
ξ [°]	0	2	-2	1.37
f	0.031	0.036	0.026	0.0302

[Title Page](#)
[Abstract](#)
[Introduction](#)
[Conclusions](#)
[References](#)
[Tables](#)
[Figures](#)
[⏪](#)
[⏩](#)
[◀](#)
[▶](#)
[Back](#)
[Close](#)
[Full Screen / Esc](#)
[Printer-friendly Version](#)
[Interactive Discussion](#)

**PRACTISE – Photo
Rectification And
ClassificaTion
SoftwarE (V.1.0)**

S. Härer et al.

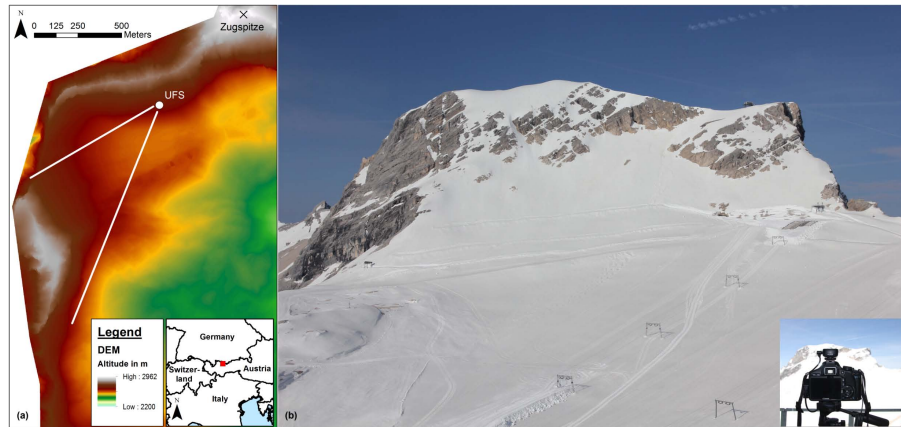


Fig. 1. (a) The test site of PRACTISE is located at the Schneefernerkopf which is situated in southern Germany, at the border to Austria (right frame). The DEM has a spatial resolution of 1 m and depicts the Zugspitze, the UFS and the field of view of the camera. (b) The digital camera system (right frame) has been installed at the UFS (2665 m a.s.l.) on 10 May 2011. The camera records hourly photographs of the investigation area, the northeastern slope of the Schneefernerkopf summit (upper central area).

[Title Page](#)[Abstract](#)[Introduction](#)[Conclusions](#)[References](#)[Tables](#)[Figures](#)[⏪](#)[⏩](#)[◀](#)[▶](#)[Back](#)[Close](#)[Full Screen / Esc](#)[Printer-friendly Version](#)[Interactive Discussion](#)

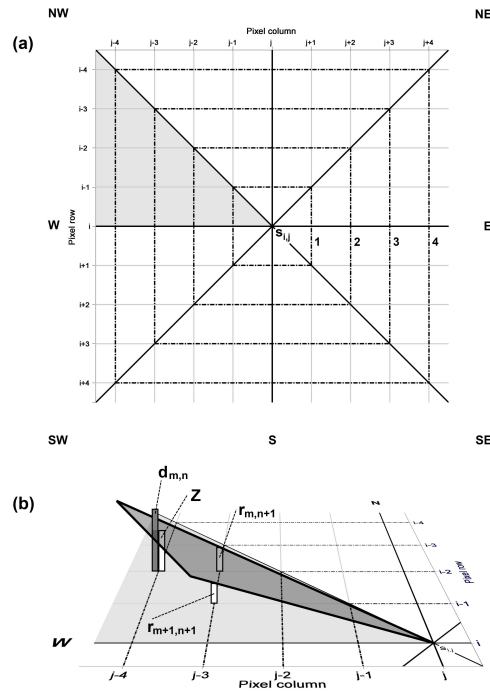


Fig. 2. (a) The viewshed calculation is divided in 8 sectors (e.g. grey-shaded W-NW sector) and main directions using the eight compass directions (N, NE, E, SE, S, SW, W and NW, black lines) from the point $s_{i,j}$. The DEM pixels are attributed to a certain ring (1, 2, 3, 4, ..., black dotted lines) depending on the distance to $s_{i,j}$. (b) The “reference planes” concept of Wang et al. (2000) is evaluated subsequently from the inner to the outer rings and is shown for an example in the 4th ring of the W-NW sector. The normalised viewpoint $s_{i,j}$, as well as the neighbouring pixels $r_{m,n+1}$ and $r_{m+1,n+1}$ (3rd ring) create a plane that checks if the pixel with the normalised elevation value $d_{m,n}$ is visible. In this case, $d_{m,n}$ is visible as the plane height Z at row m and column n is lower (adapted from Wang et al., 2000).

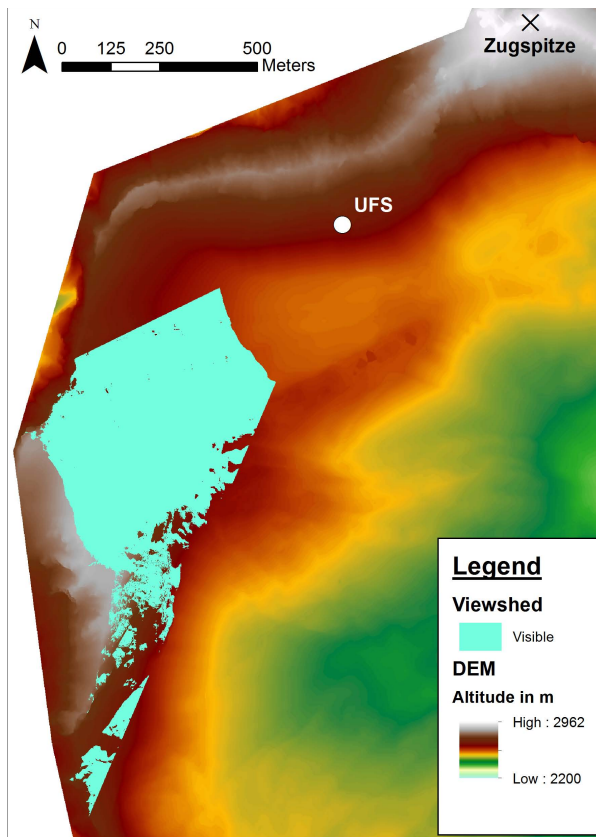


Fig. 3. The optional viewshed feature of PRACTISE computes the visible pixels (cyan) using the corresponding camera location and orientation at the UFS.

PRACTISE – Photo Rectification And Classification Software (V.1.0)

S. Härer et al.

[Title Page](#)

[Abstract](#)

[Introduction](#)

[Conclusions](#)

[References](#)

[Tables](#)

[Figures](#)

[⏪](#)

[⏩](#)

[◀](#)

[▶](#)

[Back](#)

[Close](#)

[Full Screen / Esc](#)

[Printer-friendly Version](#)

[Interactive Discussion](#)



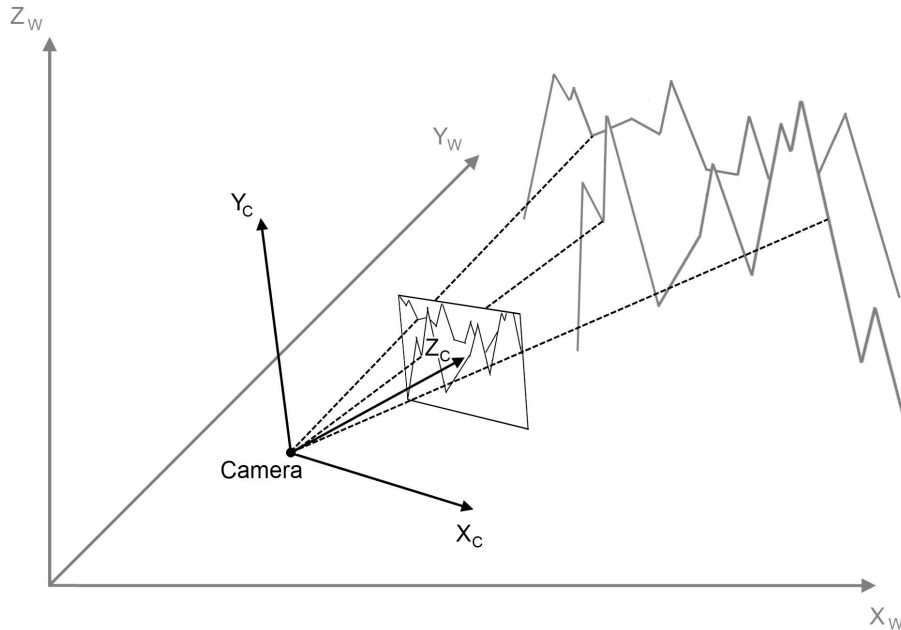


Fig. 4. The principle of the georectification procedure is as follows: at first, the mountain massif in the real world coordinate system (XYZ_W, grey) is translated and rotated to the camera coordinate system (XYZ_C, black) . Then, the 3-D mountain landscape is projected to a 2-D virtual camera image (black frame) utilizing the central projection of the camera lens (adapted from Corripio et al., 2004).

Title Page	
Abstract	Introduction
Conclusions	References
Tables	Figures
⏪	⏩
◀	▶
Back	Close
Full Screen / Esc	
Printer-friendly Version	
Interactive Discussion	

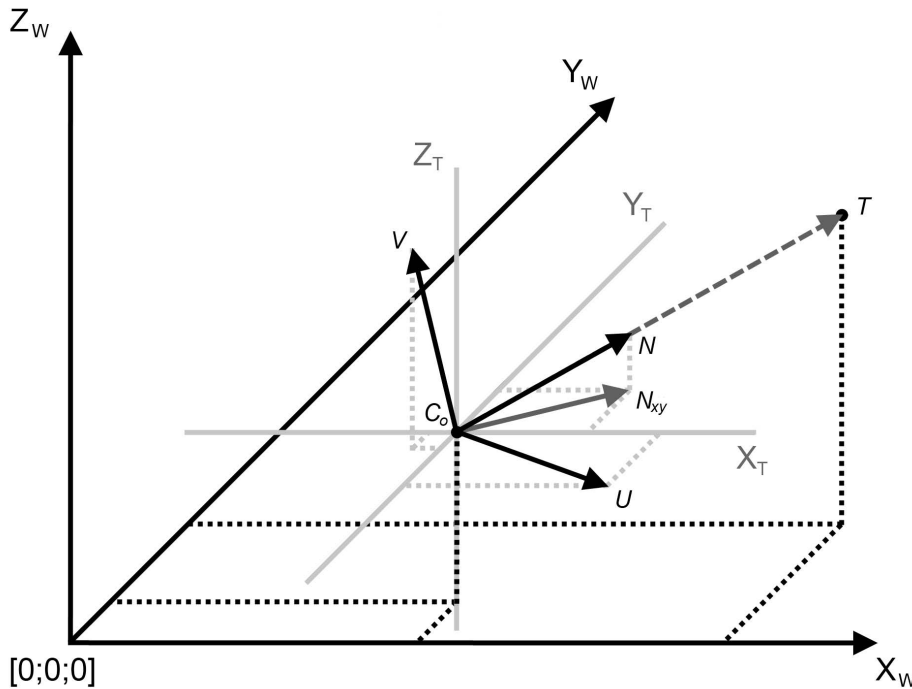


Fig. 5. The mathematical components of the translation and rotation of the real world coordinate system (XYZ_W , black) can be derived using vector calculus. The translated real world coordinate system (XYZ_T , light grey) is determined by setting C_o as coordinate system origin. The connection line from C_o to T forms the vector of the viewing direction which is subsequently normalised (N). The unit vector U is derived by the cross product of N and the unit vector of N_{xy} (dark grey) where N_{xy} is the projection of N to the XY_T plane. The directions of the camera coordinate system (black) are spanned by N , U and V where V is the cross product of U and N (adapted from Corripio, 2004).

Title Page	
Abstract	Introduction
Conclusions	References
Tables	Figures
⏪	⏩
◀	▶
Back	Close
Full Screen / Esc	
Printer-friendly Version	
Interactive Discussion	

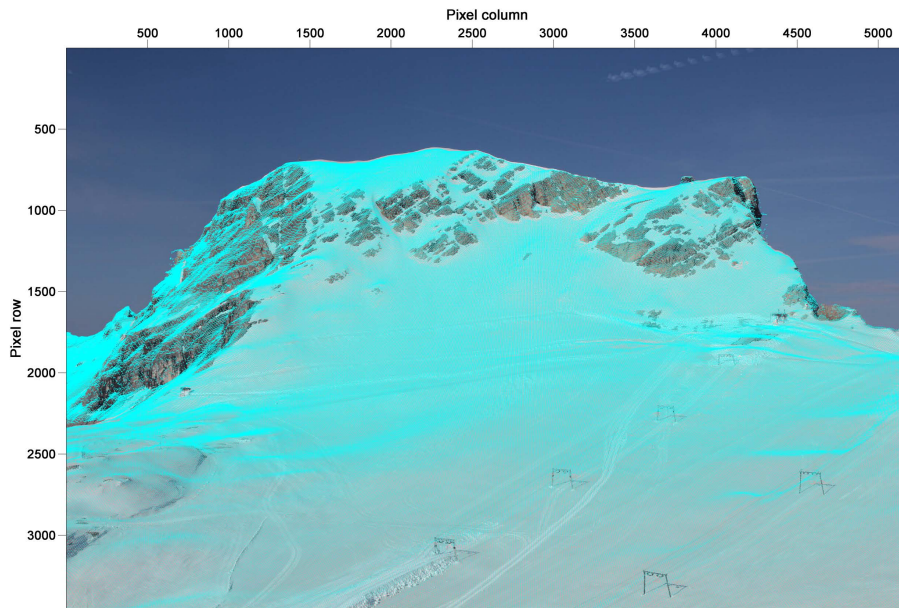


Fig. 6. The georectification of the visible DEM pixels (Fig. 3) is superimposed with cyan dots on the corresponding photograph.

PRACTISE – Photo Rectification And Classification Software (V.1.0)

S. Härer et al.

[Title Page](#)

[Abstract](#)

[Introduction](#)

[Conclusions](#)

[References](#)

[Tables](#)

[Figures](#)



[Back](#)

[Close](#)

[Full Screen / Esc](#)

[Printer-friendly Version](#)

[Interactive Discussion](#)



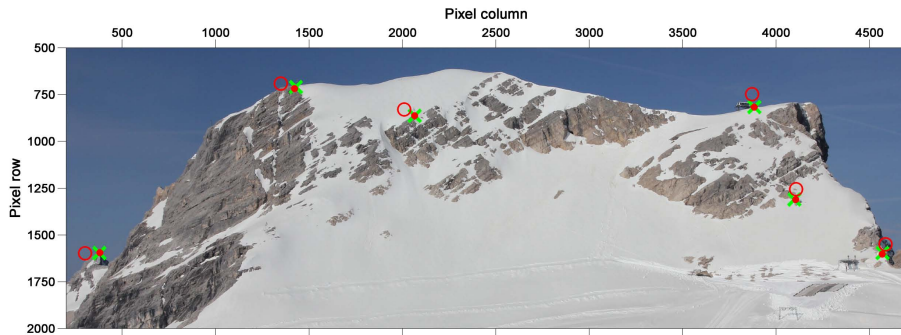


Fig. 7. The correct GCP positions are depicted as green crosses in the enlarged view of the photograph. The georectification using x^0 is shown by the red circles while the red dots illustrate the georectification after the DDS optimisation ($m = 3000$) using x^{best} .

PRACTISE – Photo Rectification And Classification Software (V.1.0)

S. Härer et al.

Title Page	
Abstract	Introduction
Conclusions	References
Tables	Figures
⏪	⏩
◀	▶
Back	Close
Full Screen / Esc	
Printer-friendly Version	
Interactive Discussion	

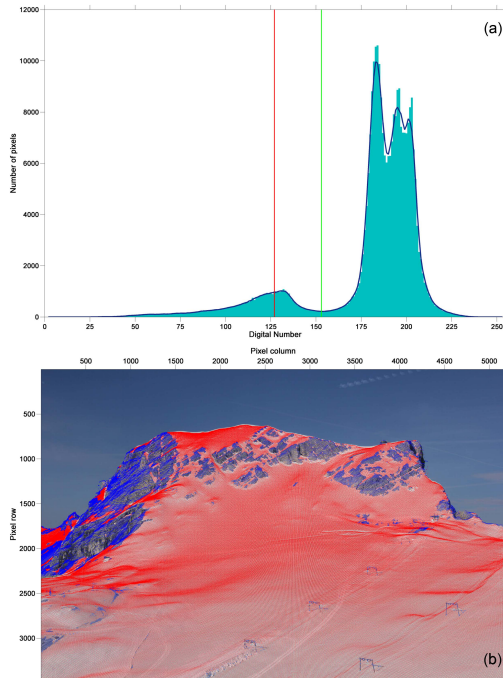


Fig. 8. (a) The automatic snow classification in PRACTISE creates a DN frequency histogram of the blue band values (blue-green bars) of the superimposed DEM pixel positions (Fig. 6). The distribution is smoothed with a moving average window size of 5 (blue line) and the snow threshold (green line) is selected for the first local minimum beyond a $DN \geq 127$ (red line). **(b)** In the overlay, all DEM pixels with a DN in the blue band in the range from the snow threshold to 255 are classified as snow (red dots), while all other pixels are assigned as no snow (blue dots).

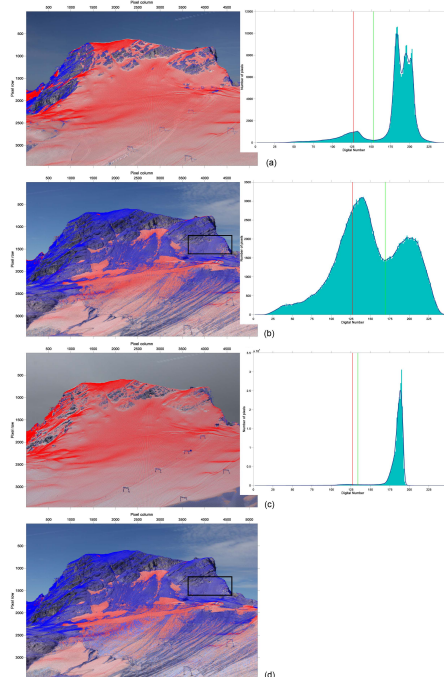


Fig. 9. The superimposition of the DEM pixels (red dots = snow, blue dots = no snow) over the corresponding photograph are shown on the left for the automatically classified images under clear sky conditions in spring on 11 May 2011 at 08:15 a.m. **(a)**, under clear sky conditions in summer on 16 August 2011, 11:05 a.m. **(b)**, and under cloudy conditions in winter on 17 February 2012 at 03:07 p.m. **(c)**, as well as for the manually processed classification of the August image. On the right, the corresponding snow thresholds (green lines) are illustrated: 153 **(a)**, 169 **(b)** and 134 **(c)**. The manual snow classification threshold is 169 for all three RGB bands and 10 for the maximum-minimum test **(d)**.

PRACTISE – Photo Rectification And Classification Software (V.1.0)

S. Härer et al.

[Title Page](#)

[Abstract](#) [Introduction](#)

[Conclusions](#) [References](#)

[Tables](#) [Figures](#)

[⏪](#) [⏩](#)

[◀](#) [▶](#)

[Back](#) [Close](#)

[Full Screen / Esc](#)

[Printer-friendly Version](#)

[Interactive Discussion](#)



PRACTISE – Photo Rectification And Classification Software (V.1.0)

S. Härer et al.

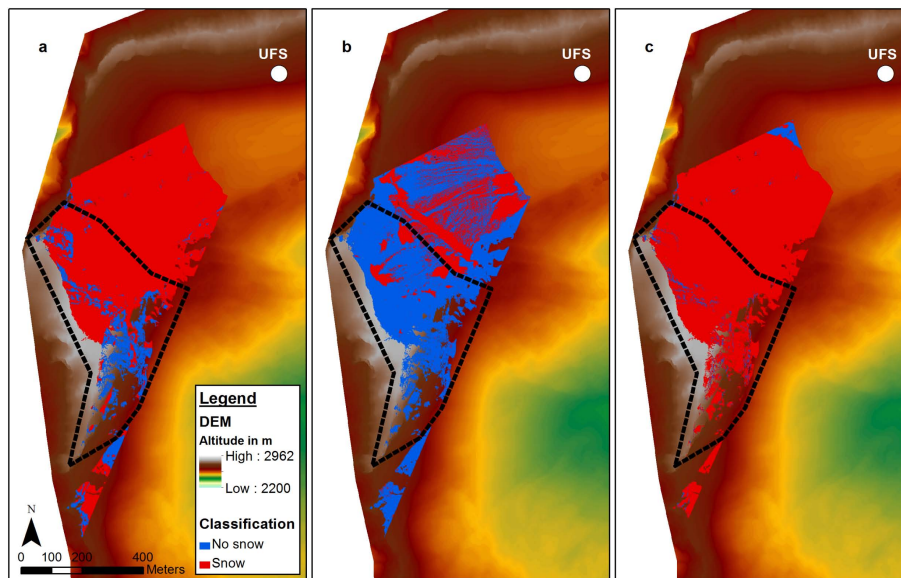


Fig. 10. The maps depict the resulting snow cover extent of the Fig. 9a (a), 9d (b), and 9c (c). The black dashed line outlines the investigation area at the Schneefernerkopf.

Title Page

Abstract

Introduction

Conclusions

References

Tables

Figures

⏪

⏩

◀

▶

Back

Close

Full Screen / Esc

Printer-friendly Version

Interactive Discussion